frontiers in Earth Science

ORIGINAL RESEARCH
published: 23 March 2022
doi: 10.3389/feart.2022.870299

A Novel Method for Estimating Model Parameters From Geophysical Anomalies of Structural Faults Using the Manta-Ray Foraging Optimization

Ubong C. Ben[1], Stephen E. Ekwok[1], Ogiji-Idaga M. Achadu[2], Anthony E. Akpan[1], Ahmed M. Eldosouky[3], Kamal Abdelrahman[4] and David Gómez-Ortiz[5]*

[1]Department of Physics, University of Calabar, Calabar, Nigeria, [2]Department of Geology, University of Calabar, Calabar, Nigeria, [3]Geology Department, Faculty of Science, Suez University, Suez, Egypt, [4]Department of Geology and Geophysics, College of Science, King Saud University, Riyadh, Saudi Arabia, [5]Department of Biology and Geology, Physics and Inorganic Chemistry, ESCET, Universidad Rey Juan Carlos, Madrid, Spain

The Manta-Ray Foraging Optimization has been adapted and implemented in computing model parameters from potential field anomalies originating from two-dimensional dipping faults. The inversion technique was originally demonstrated on magnetic anomalies from uncorrupted–then, corrupted synthetic datasets. Thereafter, it was experimented on profiles taken from mining fields in the United States, and Australia. The results obtained showed that the design procedure is admirably stable and flexible, especially when dealing with noisy data. It is also notably efficient in the quantitative resolution of geophysical inverse problems. The consistency in results obtained from analysis of deep-seated and shallow field examples, even when compared against background results, is also impressive. The new technique has also exhibited notable superiorities over other well-known and conventional techniques, especially on the grounds of convergence rate, cost, and quality of resolved anomaly parameters. Consequently, it is recommended for interpretation of other structures and modeling of other geophysical data like self-potential and resistivity data.

Keywords: manta-ray, optimization, magnetics, gravity, Fault

OPEN ACCESS

Edited by:
Mourad Bezzeghoud,
Escola de Ciência e Tecnologia,
Universidade de Évora, Portugal

Reviewed by:
Serdar Ekinci,
Batman University, Turkey
Qiang Guo,
China Jiliang University, China
Kittisak Jermsittiparsert,
Dhurakij Pundit University, Thailand

****Correspondence:***
Ahmed M. Eldosouky
dr_a.eldosoky@yahoo.com

Specialty section:
This article was submitted to Solid Earth Geophysics, a section of the journal Frontiers in Earth Science

Received: *06 February 2022*
Accepted: *28 February 2022*
Published: *23 March 2022*

Citation:
Ben UC, Ekwok SE, Achadu O-IM, Akpan AE, Eldosouky AM, Abdelrahman K and Gómez-Ortiz D (2022) A Novel Method for Estimating Model Parameters From Geophysical Anomalies of Structural Faults Using the Manta-Ray Foraging Optimization. Front. Earth Sci. 10:870299. doi: 10.3389/feart.2022.870299

INTRODUCTION

In magnetics and gravity prospecting, signals of interest typically include those originating from buried rock units, as well as those from neighboring formations. The interpretational focus, however, is mostly on geologic structures that are of economic end-importance. Faults, ores, contacts, and dykes are examples of such structures. Notably, attention on the interpretation of anomalies due to faults for mineral prospecting has been appreciated among geophysicists lately. This is unrelated to the fact that over the years–in addition to immense improvements in geophysical data interpretation measures; faults have proven as good traps and caps over hydrocarbon pools. They have also been known to exert a strong influence on the regional and local direction of mineralization (Li et al., 2020).

Several techniques that ensure economically friendly and accurate acquisition and processing of potential field data have been developed and accepted for different exploration problems. However, for optimal interpretability and also to ensure the suitability of the acquired data for structural

imaging of the subsurface, the data must undergo geophysical inversion (Abo-Ezz & Essa, 2016). Geophysical inversion is a step-by-step modeling approach that aims to unravel the features of buried geologic structures by establishing similarities between them and to already well-defined models (Essa & Munschy 2019). Over the years, various inversion techniques have been designed for the deciphering/computation of these characteristic physical parameters. Some of these procedures are united by adept functional exploitation of computational approaches including Euler deconvolution (Mota et al., 2020), Werner deconvolution (Cerovský & Pašteka 2003), model layering (Pilkington 2006), and parametric curves (Abdelrahman et al., 2012). Others employ procedures consistent with fair function minimization and Depth From Extreme Points (DEXP) (Abbas and Fedi 2013), simplex algorithm (Pan et al., 2009), and linear least squares (Melo & Barbosa 2018). However, experience has shown that results obtained from these conventional inversion approaches usually lead to the generation of large amounts of invalid solutions. The invalid solutions are caused by many factors including noise sensitiveness and poor window size compatibility (Li et al., 2020). Another cause is improper filtering of noise from signals of interest. Also, there is a characteristic over-dependence of initializations on subjective priori geologic information which may not be reliable or sufficiently reputable.

With recent improvements in machine intelligence, these classical magnetic inversion methods are gradually being substituted with more dependable, accurate, and reliable metaheuristic techniques. Some of the intelligent techniques employed for geophysical inversion include ant colony optimization - ACO (Gupta et al., 2013); genetic algorithm (Sen & Mallick 2018), particle swarm optimization- PSO (Guo et al., 2020; Essa 2021; Essa et al., 2021); neural networks method (Yadav et al., 2021); differential evolution-DEA (Garabito and Cruz 2019; Ekinci Y. L. et al., 2021); simulated annealing (Pan et al., 2009) and genetic price algorithm (Kaftan 2017). These intelligent algorithms, which mostly work by the functional imitation of the normal behavior of objects from nature; have generally upset most of the challenges posed by the classical algorithms. The most obvious advantage of these techniques is that they are conditioned to be zero-ordered. This implies that any performance enhancements made in a direction towards feasible solutions are not related to the derivatives of the function minimized/maximized.

The performance of the above-mentioned intelligence-based methodologies have generally been applausive. This is especially in terms of optimized structural resolvability and improvements in interpretation quality. Howbeit, these methodologies are still short of analytical perfection, particularly in terms of convergence and computational cost (Hemeida et al., 2020; Ben et al., 2021b; Mbonu et al., 2021; Turgut 2021). Continual pursuit of this analytical perfection necessitates continual development and deployment of new optimizers and hence, the motivation for this study. In this research paper, we present a new way of parameterizing magnetic and gravity anomalies generated by dipping fault structures based on the Manta-Ray Foraging Optimization (MRFO) algorithm.

The MRFO algorithm—a relatively recent metaheuristic technique, leverages the bio-inspired foraging strategies of Manta-Rays for the resolution of optimization problems (Hemeida et al.., 2020). The MRFO approach has previously been tested and proven to be effective with contextual and engineering challenges such as Covid-19 thresholding, arrhythmia classification, energy minimization, wind turbine control, fractional-order proportional–integral–derivative controller design as well as magnetic levitation system (Ekinci et al., 2021b; Ekinci et al., 2021c; Feng et al., 2021; Houssein et al., 2021; Rezk et al., 2021). From the results of those applications, MRFO optimization technique was reported as superior to existing heuristic algorithms in several ways, such as better accuracy, enhanced performance, and lower computational cost. Resultantly, the scholars strongly recommended the method for inversion situations. Up to the initial draft of this manuscript, a total of two geophysical inversion studies using the MRFO technique has been reported in published literature. Ben et al. (2021b) employed the technique for the modeling of dipping dykes; Ben et al. (2021c) interpreted gravity anomalies over geometric geological structures such as spheres, cylinders, sheets, and, horizontal faults using the MRFO strategy. Barnhart and Lohman (2010), Amoruso et al. (2013), and, Qureshi & Nalaye (1978) have however explained problems associated with interpreting faults without regards to the angle of dip–especially for fault structures in highly deformed regions, e.g zones of folding. The novelty of this study lies in the pioneering application of the MRFO algorithm to non-horizontal fault problems. The parameters sought in this study are those defining the character, location, and position of the subsurface feature. The new method presents a couple of merits. First, unlike deterministic schemes, iterative computations are independent of the gradient of the objective function, technically limiting immature convergence. Also, the wild function injected during the cyclone foraging stage of the algorithm design allows initial models to parameterize from anywhere within a size-independent range (as would be seen in the examples)—reducing reliance on subjectivity. Most importantly, the superiority of the MRF tool actually lies with its foraging character. With MRFO algorithm, the search agents are allowed to switch intelligently and at any point between the strategies of chain foraging and cyclone foraging. The chain foraging behavior allows significant local search while the cyclone foraging behavior concurrently assures non-deterioration of global search during the process; a mutualization of the two as allowed by the new technique ensures comparatively quality solutions through a thorough exploration of the whole domain of the geophysical problem.

The layout of the present paper is described as follows. First, the 2-D potential field problem with respect to dipping faults is introduced. Next, the proposed inversion methodology based on MRFO is strategically constructed. The technique is then experimented on synthetically constructed models corrupted with random noise at varying levels and further, with two real case studies. The obtained parameter values are then compared with published results previously reported for similar anomalies but obtained using other conventional techniques. Additionally,

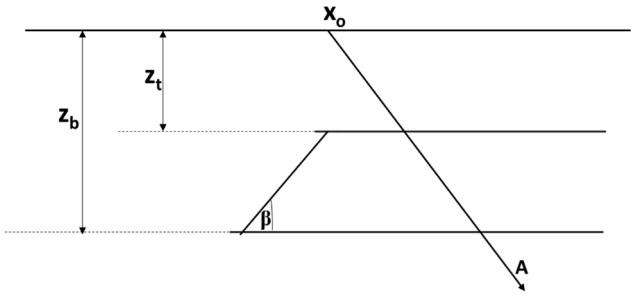

FIGURE 1 | A dipping fault model.

to understand uncertainties in the obtained solutions, appraisals are conducted using Markov Chain Monte Carlo sampling procedure. The MCMCprocedure adopted employs the simulated-annealing without cooling scheme. Finally, the study concludes with a brief assessment of the applicability and effectiveness of MRFO as a tool for inversion of gravity and magnetic field anomalies.

METHODOLOGY

Forward Modeling Problem

Assume a standard Cartesian coordinate system whose ordinate represents the strike of a dipping fault buried at depth z, and whose abscissa indicates the profile direction (**Figure 1**). The magnetic -T and gravity G anomalies- (collectively depicted as P later in the paper for inclusiveness and generality) (**Eq. 1** and **Eq. 2**); of the two-dimensional fault at any point x_k can be expressed as (Essa, 2013; Abdelrahman et al., 2019):

$$G(x_k, A, x_o, z, \beta) = A\left[\pi + \tan^{-1}\left(\frac{x_k - x_o}{z_t} + \cot\beta\right) - \tan^{-1}\left(\frac{x_k - x_o}{z_b} + \cot\beta\right)\right], \quad (1)$$

$$T(x_k, A, x_o, z_t, z_b, \beta) = A\left[\sin\beta\left(\tan^{-1}\frac{x_k - x_o}{z_t} - \tan^{-1}\frac{x_k - x_o}{z_b}\right) + \frac{\cos\beta}{2}\left(\ln\frac{(x_k - x_o)^2 - z_b^2}{(x_k - x_o)^2 - z_t^2}\right)\right], \quad (2)$$

where z_t is depth to the top and z_b is depth to the bottom of the structure from the observation plane, β and A are respectively, the dip angle, and amplitude coefficient that has a direct relationship with thickness of fault, density contrast of the gravity anomaly case and inclination of the geomagnetic field in the vertical plane perpendicular to the strike of the fault.

These five controlling model parameters were determined in this research, by constraining the cost function—*obj* (**Eq. 3**) using the MRFO procedure. Acceptable values were determined by lessening disparities between the calculated and actual data (Essa et al., 2018; Ekinci et al., 2019).

$$objective\ function = \frac{\sum_{i=1}^{S}\left(P_i^m - P_i^c\right)^2}{S}, \quad (3)$$

where P_i^m and P_i^c are respectively the potential field anomaly from observed data and those estimated using the proposed methodology.

Manta-Ray Foraging Optimization Algorithm

Manta-Rays, one of the ocean's biggest creatures, are commonly found in tropical environments. As manta-rays are naturally toothless (**Figure 2**), their diet is normally limited to microscopic aquatic creatures -planktons (Alturki et al., 2020). Due to the dependence of plankton on ebbs and tides, the occurrence of planktons in large concentrations is often erratic and infrequent. For that reason, finding the best strategies for assuring consistent food availability is essential for Manta-Ray survival (Izci et al., 2020). Interestingly, Manta-Rays have developed and honed several clever foraging tactics that are so effective they rarely face food scarcity. The MRFO algorithm, which provides the basis of our new methodology, is premised on these distinct foraging strategies, specifically the chain, somersault, and cyclone techniques (Turgut, 2021). Herewith, vectorial positions of each foraging Manta-ray depict probable positions of the required potential field parameter; and that of the planktons indicate the optimum solution to the geoscientific problem. The accompanying sections discuss these foraging approaches as well as the numerical constructs designed for our novel geophysical methodology.

Chain Foraging

Manta-Rays implement the chain foraging method by first, locating prospective plankton and then, advancing toward it via a foraging chain (technically a head-tail formation). As a result, the neighbor would immediately take up any plankton

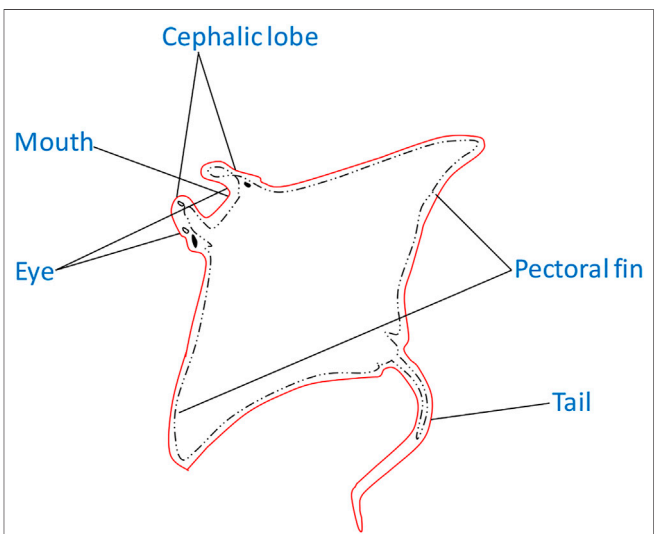

FIGURE 2 | Simplified anatomy of a Manta-Ray.

that is missed by one agent and improve overall opportunities for exploitation. The denser the concentration of plankton at a specific position, the stronger that position (Ghosh et al., 2021; Houssein et al., 2021). To achieve this strategy a premise equating the original best position to the current optimal solution is employed. This comparative position was subsequently utilized to update the location of each agent and its immediate predecessor. For our dipping fault problem, the strategy was implemented using **Eq. 4** (Houssein et al., 2021).

$$P(\mathrm{x}_k) = \begin{cases} \mathrm{P}(\mathrm{x}_k)_i^4(t) + \boldsymbol{r}.(\mathrm{P}(\mathrm{x}_k)_{best}^4(t) - \mathrm{P}(\mathrm{x}_k)_i^4(t)) + \boldsymbol{w}.(\mathrm{P}(\mathrm{x}_k)_{best}^4(t) - \mathrm{P}(\mathrm{x}_k)_i^4(t)) \boldsymbol{i} = 1 \\ \mathrm{P}(\mathrm{x}_k)_i^4(t) + \boldsymbol{r}.(\mathrm{P}(\mathrm{x}_k)_{i-1}^4(t) - \mathrm{P}(\mathrm{x}_k)_i^4(t)) + \boldsymbol{w}.(\mathrm{P}(\mathrm{x}_k)_{best}^4(t) - \mathrm{P}(\mathrm{x}_k)_i^4(t)) \boldsymbol{i} = 2, 3, \ldots, \boldsymbol{T} \end{cases}, \tag{4}$$

$$\boldsymbol{w} = 2.\boldsymbol{rand}().\sqrt{|\log(\boldsymbol{r})|}, \tag{5}$$

where $\mathrm{P}(\mathrm{x}_k)(t)$ is search agent's *i*th position (the potential field parameters) at t, T the maximum iteration number; w the weight coefficient (**Eq. 5**); *rand*()-a vector randomly generated between 0 and 1 while $\mathrm{P}(\mathrm{x}_k)_{best}^4(t)$ the optimal geophysical parameter position vector is technically located in the healthiest plankton cluster.

The *i*th individual's position is determined by positions $\mathrm{P}(\mathrm{x}_k)_{i-1}^4(t)$ of the (i-1)$^{\text{th}}$ search agent and $\mathrm{P}(\mathrm{x}_k)_{best}^4(t)$ of the food (the target solution of our geophysical problem).

Cyclone Foraging

If a group of Manta-Rays, as detailed above, identify and create a foraging chain to lucrative plankton in deep water, they will glide towards them in spirals. The spirals are similar to the one employed in the Water Optimization Algorithm (Gharehchopogh & Gholizadeh 2019). For MRFO, however, the approaching Manta-Ray swarm maintains their line while whirling, such that while an individual follows the one in front, it is still going towards the target food.

We use the following equations to numerically describe this method in a form that is specific to our potential field problem (Zhao et al., 2020).

$$\mathrm{P}(\mathrm{x}_k)_i^4(\boldsymbol{t}+1) = \begin{cases} \mathrm{P}(\mathrm{x}_k)_{best}^4(t) + \boldsymbol{rand}().(\mathrm{P}(\mathrm{x}_k)_{best}^4(\boldsymbol{t}) - \mathrm{P}(\mathrm{x}_k)_i^4(\boldsymbol{t})) + \boldsymbol{w}.(\mathrm{P}(\mathrm{x}_k)_{best}^4(\boldsymbol{t}) - \mathrm{P}(\mathrm{x}_k)_i^4(\boldsymbol{t}))\boldsymbol{i} = 1 \\ \mathrm{P}(\mathrm{x}_k)_{best}^4(t) + \boldsymbol{rand}().(\mathrm{P}(\mathrm{x}_k)_{i-1}^4(\boldsymbol{t}) - \mathrm{P}(\mathrm{x}_k)_i^4(\boldsymbol{t})) + \boldsymbol{w}.(\mathrm{P}(\mathrm{x}_k)_{best}^4(\boldsymbol{t}) - \mathrm{P}(\mathrm{x}_k)_i^4(\boldsymbol{t}))\boldsymbol{i} = 2, 3, \ldots, \boldsymbol{T} \end{cases}, \tag{6}$$

where w is asymptotically generated by **Eq. 7** as weight coefficient for cyclone foraging.

$$w = 2e^{rand()\frac{T-t+1}{T}}\sin 2\pi rand(), \tag{7}$$

However, after completing this stage successfully, the estimations for the required fault parameters failed to converge repeatedly and instead become unstable; fluctuating about a central position inside the search space. Convergence was obliged by nudging each agent to new positions that differed from their current ones but remained within the problem domain. This was strategized by injecting a wild random function into each structural parameter's bound (Houssein et al., 2021; Ghosh et al., 2021). This local strategy allowed comprehensive global search by MRFO and significantly increased overall exploration. The numerical construct for this stage is expressed as shown in **Eq. 8**. It was generically implemented using **Eq. 9** (Rezk et al., 2021).

$$\boldsymbol{q}_{\boldsymbol{rand}}^4 = \boldsymbol{LB}^4 + \boldsymbol{rand}().\left(\boldsymbol{UB}^4 - \boldsymbol{LB}^4\right), \tag{8}$$

$$\mathrm{P}(\mathrm{x}_k)_i^4(t+1) = \begin{cases} \boldsymbol{q}_{\boldsymbol{rand}}^4(t) + \boldsymbol{rand}().\boldsymbol{q}_{\boldsymbol{rand}}^4(t) - \mathrm{P}(\mathrm{x}_k)_i^4(t)) + \boldsymbol{\mu}.(\boldsymbol{q}_{\boldsymbol{rand}}^4(t) - \mathrm{P}(\mathrm{x}_k)_i^4(t))\boldsymbol{i} = 1 \\ \boldsymbol{q}_{\boldsymbol{rand}}^4(t) + \boldsymbol{rand}().(\mathrm{P}(\mathrm{x}_k)_{i-1}^4(t) - \mathrm{P}(\mathrm{x}_k)_i^4(t)) + \boldsymbol{\mu}.(\boldsymbol{q}_{\boldsymbol{rand}}^4(t) - \mathrm{P}(\mathrm{x}_k)_i^4(t))\boldsymbol{i} = 2, 3, \ldots, \boldsymbol{T} \end{cases}, \tag{9}$$

where $\boldsymbol{q}_{\boldsymbol{rand}}^4$ is the random function explained earlier.

Somersault Foraging

Here, the search domain is reconstructed such that our ideal geophysical solution (promising planktons) is positioned as a pivot. This is such that, before somersaulting off to other locations, each of our investigative search agents revolves around this pivot. By this, the new positions are not completely random or stray too far, but rather circle about the most promising found up to that time. With increasing iterations, the algorithm is designed such that the somersaulting range is intelligently lowered step-wise until the solutions are obtained. This is achieved numerically using **Eq. 10** (Elattar et al., 2020; Ben et al., 2021b; Feng et al., 2021)

$$\begin{aligned} \mathbf{P}(\mathbf{x}_k)_i^4(\boldsymbol{t}+1) = \mathbf{P}(\mathbf{x}_k)(\boldsymbol{t}) + \boldsymbol{S}.\boldsymbol{rand}_1().\mathbf{P}(\mathbf{x}_k)_i^4(\boldsymbol{t}) \\ - \boldsymbol{rand}_2().\mathbf{P}(\mathbf{x}_k)_i^4(\boldsymbol{t}), \\ \boldsymbol{i} = 1, 2, \ldots, \boldsymbol{N}, \end{aligned} \tag{10}$$

where the term S—a constant known as the somersault factor, determines the Manta-Ray's somersaulting range. $rand_1()$ and $rand_2()$ determined randomly between 0 and 1 were generated using PYTHON's NUMPY library.

Random initialization of the Manta-Ray's population in the search space (designed around the UB and LB) is the first step in our proposed method. Each agent in the domain is made to contain all the fault parameters required. The user-selection of UB and LB for each structural problem is driven by historical geology, geophysical, and petrophysical information. The bounds do not necessarily affect the results but only prevent the agents from completely iterating out into infinity. At each iteration step, the agents update their current positions based on the agent preceding them and their referential position. These positions of reference are determined by t/T, whose value is skillfully decreased from 1/T to 1 for exploratory and exploitative searches (Houssein et al., 2021). Exploitation is done when t/T is smaller than rand(); otherwise, exploration takes place. As a result, the MRFO algorithm enables individuals to determine and, if necessary, transpose between cyclone and chain behaviors. These calculations and updates are carried out iteratively, step by step, until the stopping criterion is met.

The estimated data was assessed after each step by comparing it with the measured data using RMS error technique (**Eq. 3**).

The best positions representing the five required model parameters are returned whenever convergence is achieved. **Figure 3** is a flowchart for the entire optimization procedure discussed above.

Algorithm Configuration/Time Complexity

The algorithm used for this study was designed with PYTHON3 programming package and compiled on the VSCode developer

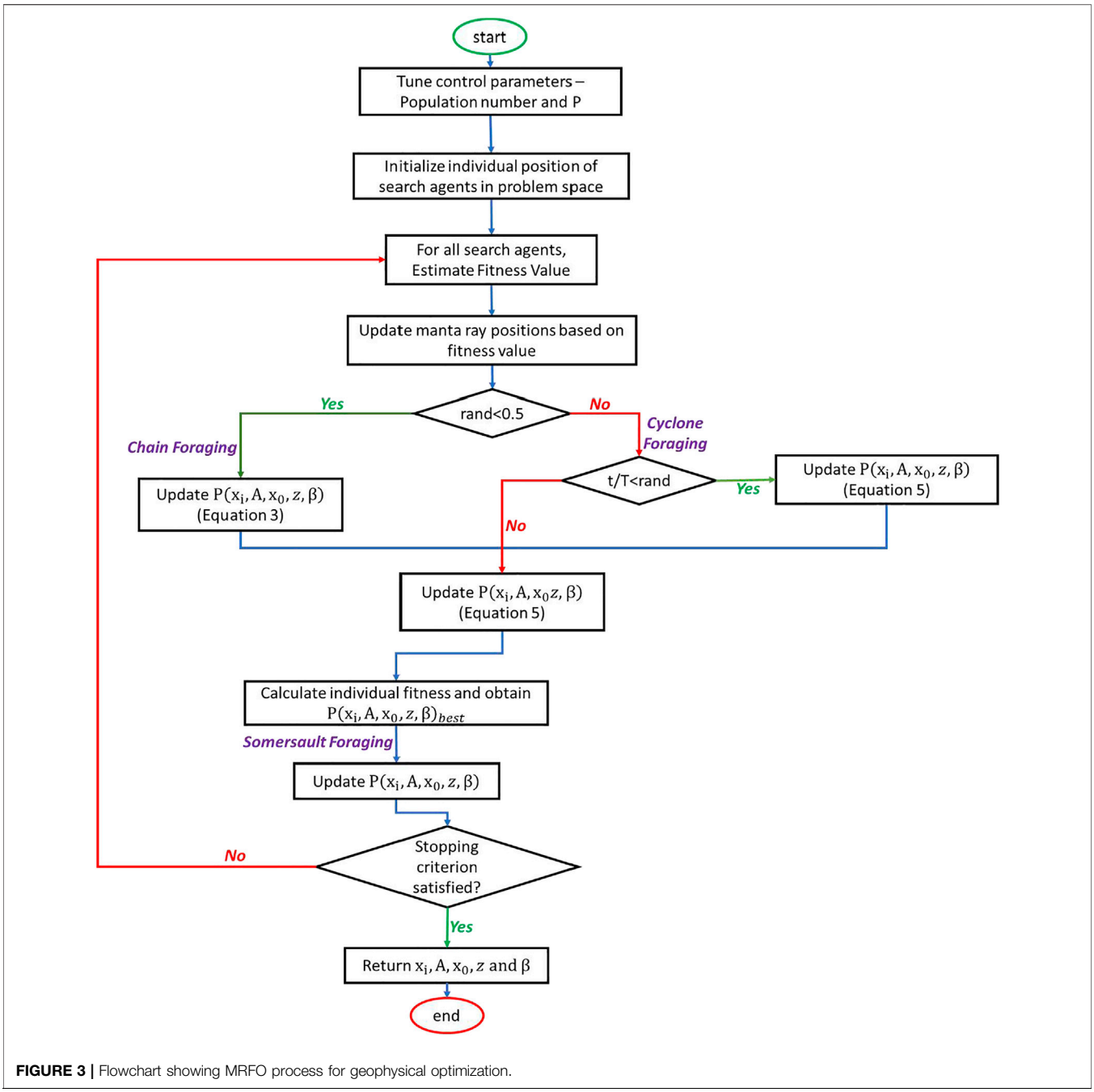

FIGURE 3 | Flowchart showing MRFO process for geophysical optimization.

environment. The compiling environment was installed on a simple PC running on a core i7 processor and a Windows 10 package.

For time complexity, this factor depended-first on the structural feature's complexity; then on the number of iterations allowed. Nonetheless, for all cases in this study, the process rounded up completely in less than 50 s.

Uncertainty Analysis

Arising from the characteristic non-uniqueness, non-linearity, and ill-posedness of geophysical inverse problems; it is mathematically possible for various models constructed from different sets of parameters to fit into similar observed measurements. This situation usually raises considerable uncertainty around ultimately estimated parameters. As a result, uncertainty appraisal has come to be accepted as very vital in inversion studies (Scales & Tenorio 2001).

The Bayesian approach has been reportedly employed in parameter estimations involving considerable stochasticity. The procedure relies on the concept of conditional probability. By combining a priori information with the experimental data's likelihood, prior probability distributions for the required

parameters could be obtained (Tarantola 2005; Biswas et al., 2017; Yusof et al., 2018). For global optimization algorithms like SA, PSO, and, GA, correct sampling has been achieved with the Markov-Chain Monte Carlo algorithm (Yusof et al., 2018; Ekinci et al., 2020). For this investigation, the Metropolis-Hasting algorithm (M–H), a generalized Markov chain Monte Carlo (MCMC) method (Metropolis et al., 1953; Hastings, 1970) was used for parameter sampling. The M-H method suggests various models based on some prior distribution. The likelihood of each proposed model is computed by resolving the forward model problem and then, obtaining the misfit in the data. If there is a likelihood increase, the revised model is accepted. Nonetheless, even if there is an observed decrease in likelihood, the proposed model can still be accepted, although with a probability dependent on the ratio of likelihood between the proposed and the original model. The method, based upon simulated annealing, allowed for the assessment of uncertainty by providing parameter confidence intervals (Ekinci et al., 2020).

PARAMETER TUNING STUDIES

Pluralities of bio-inspired global optimization algorithms have unique control parameters that have a big impact on the algorithm's inversion convergence point. These control features are critical for any algorithm's overall performance. Their selection, however, heavily depends on the problem-at-hand's nature (Kanimozhi & Jacob 2019; Gonzalez et al., 2021). Resultantly and prior to conducting our inversion analysis, we modify model parameters to establish the appropriate control parameters for the Manta-Ray algorithm. The parameter tuning study in our metaheuristic instance is primarily concerned with determining the optimum population of experimenting agents and the Somersault factor–S.

To properly guide the tuning studies, a synthetic magnetic anomaly dataset was theoretically generated using **Eq. 1** with A = 200 nT. Further, z_b = 30 m, z_t = 10 m, $\beta = 40^{\circ}$, x_o = 10 m, and profile length was 160 m. A synthetic gravity anomaly dataset was also generated with A = 50 mGal, z_b = 30 m, z_t = 8 m, $\beta = 40^{o}$, x_o = 0 m, and profile length of 80 m. In both synthetic magnetic and gravity data experiments, broad search spaces (**Table 1**, **2**) are adopted for the model parameters. This was to enable investigation of S's effect on the overall solution. The inversion of both anomalies was then carried out using identical approaches. Thirty independent runs in 500 optimization iterations were permitted with population number = 150. The select population number was arrived at by multiplying the number of unknown model parameters (5) with total independent runs allowed (30). The magnetic and gravitational anomaly problem was thereafter investigated statistically utilizing the mean, standard deviation, and minimum of the RMS. **Tables 3** (magnetic data) and 4 (gravity data) show the findings obtained for various S values.

According to the tables, the best statistical results (boldface) were obtained with an S value of 2. This means that using this value as the S for both gravity and magnetic data would make the whole optimization process more resilient and effective. The huge range in error values between the control producing the best and those producing the worst is another notable/interesting observation. This huge discrepancy could definitely have a significant impact on the solution's correctness in relation to the optimal model parameter resolution. This so emphasizes the critical need for parameter tuning studies during global optimization applications.

TABLE 1 | Search space, actual and estimated parameters uncorrupted synthetic gravity anomaly.

Anomaly parameters	Search Space	Actual (Control)	Estimated
A (mGal)	0–200	50.000	49.974
x_o (m)	−20–20	0.000	0.036
z_b (m)	0–100	30.000	30.278
z_t (m)	0–50	8.000	7.892
β (°)	−180–180	40.000	39.991

TABLE 2 | Bounds, actual and estimated parameters for uncorrupted synthetic magnetic anomaly.

Anomaly parameters	Search bounds	Actual (Control)	Estimated
A (nT)	0–500	200	200.031
x_o (m)	−50 – 50	10	9.931
z_b (m)	0–100	30	30.008
z_t (m)	0–100	10	10.003
β (°)	−180–180	40	39.997

TABLE 3 | Statistical results for RMS values obtained from parameter tuning of MRFO for synthetic magnetic dataset.

S	RMS (nT)		
	Minimum	Mean	Standard deviation
0.5	1.3869	1.7836	0.7548
1	0.5383	0.9471	0.2674
1.5	0.2536	0.4368	0.0734
2	0.0745	0.8352	2.4836×10^{-5}
2.5	0.1338	0.1836	5.3425×10^{-3}
3	0.3846	0.5358	0.2036

SYNTHETIC EXAMPLES

To assess performance, we put the proposed methodology through controlled series of tests using synthetic data simulating an idealized dipping fault. The uncorrupted version synthetic anomaly was examined first; then the clean anomaly was purposefully contaminated with noise and reanalyzed.

Noiseless Anomaly

The MRFO technique was used to investigate the uncontaminated magnetic and gravity field anomalies synthetically generated for a dipping fault structure. The synthetic magnetic anomaly constructed along a 160-m long

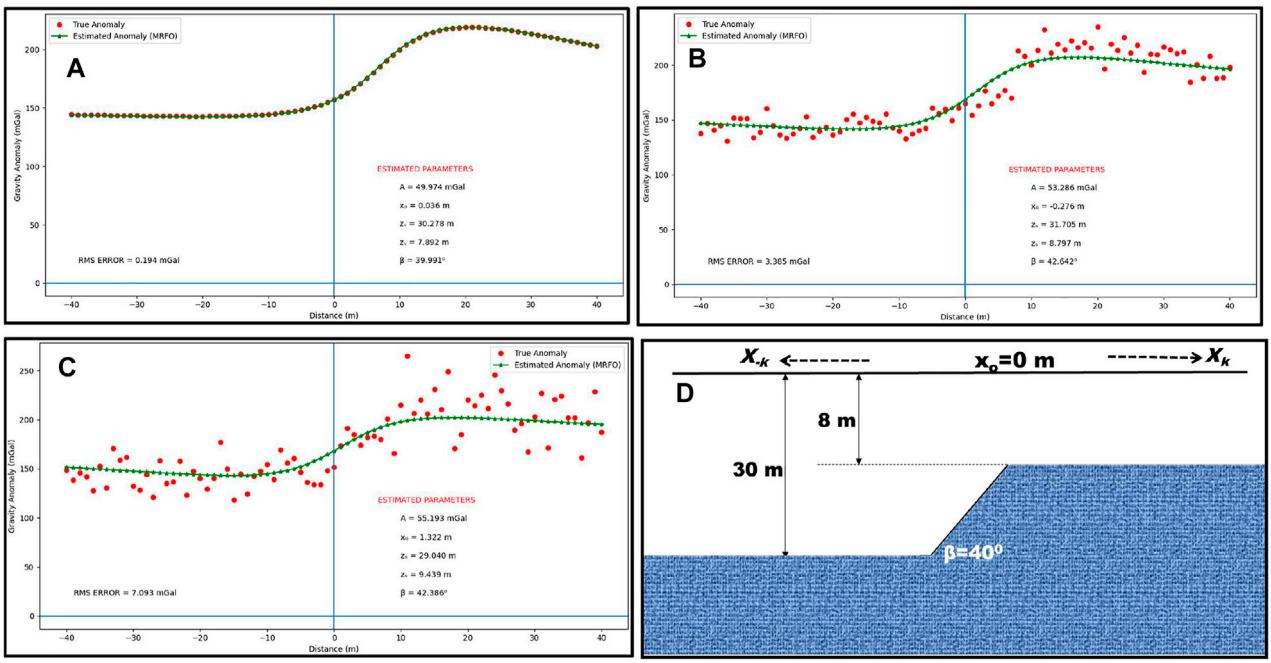

FIGURE 4 | Actual and estimated anomalies (gravity) of a synthetic dipping fault structure with **(A)** 0% **(B)** 5% **(C)** 10% Gaussian noise using MRFO algorithm **(D)** Sketch of the fault model.

profile was sampled at 1 m sampling interval. Model parameters: A = 200 nT, z_b = 30 m, z_t = 10 m, $\beta = 40^{\circ}$, x_o = 10 m was adopted. The synthetic gravity anomaly was produced with A = 50 mGal, z_b = 30 m, z_t = 8m, $\beta = 40^{\circ}$, x_o = 0 m along an 80 m profile. The gravity profile was also sampled at an interval of 1 m. The magnetic and gravity anomalies were computed with **Eqs 1**, **2** respectively.

The search space was populated with 150 initial models/vectors and a broad range of parameter boundaries. For the magnetic case, A-values were set to be in the range of 0–500 nT, and β from -180° to 180°, z_b ranged from 0 to 100 m z_t from 0 to 100 m while x_o stretched between—50 and 50 m. On the other hand, for the gravity anomaly, A was set to vary between 100 and 2000 mGal, β from −180° to 180°, z_b ranged from 0 to 100 m, z_t from 0 to 50 m, and x_o from—20 to 20 m. A total of 500 repetitive iterations were allowed for each run. MFRO has comprehensive and powerful search capabilities. Convergence was attained in less than 100 steps; and good approximations of the five model parameters (A, x_o, z_b, x_t) determined to be in good agreement with their known values were obtained (**Figures 4A**, **5A**; **Table 1**, **2**). Furthermore, a careful evaluation of the histogram generated after uncertainty appraisal analysis (**Figures 6**, **7**) reveals the estimates within highly acceptable confidence intervals.

Noisy Anomaly

To imitate non-ideal subsurface conditions, the previously modeled synthetic dataset was contaminated with varying degrees of Gaussian random noise (5 percent and 10 percent). Using a customized version of the SCIPY library, the Gaussian noise generation process was automated and then individually added data. These various amounts of noise were added to evaluate the suggested methodology's efficacy in the presence of external interferences. These interferences may be from a host material or even signals from neighboring geologic intercalations (Balkaya & Kaftan 2021; Essa & Abo-Ezz 2021). **Eq. 11** was used for calculating the noise percentage.

$$\textbf{Noise percentage} = \frac{\boldsymbol{P}_{\mathbf{n}} - \mathbf{P}}{\mathbf{P}_{\mathbf{n}}}, \tag{11}$$

where P and P_n respectively represent the clean and contaminated anomalies.

With **Eq. 3** used as the cost function, and parameter bounds identical to those used in the noiseless anomaly, cases were re-adopted; the anomalies were reanalyzed with MRFO. The misfit and their convergence were examined after each iteration.

The MRFO algorithm-estimated model parameters were found to be remarkably consistent (**Figures 4B**,C, **5B**,C; **Tables 4**, **5**). **Figures 4D**, **5D** show the Sketches of the fault models. However, based on the results, A appeared to be more sensitive to increasing noise. This sensitivity, which is likely to alter interpretations when dealing with exceedingly sophisticated and deep-seated problems, may be explained by the fact that A is a multiplier factor (**Eqs 1**, **2**). In any case, it could be easily handled by shortening the lower-upper bound range. Further, the results show that the after-convergence misfit and RMS error increase somewhat with the noise level. Nonetheless, this does not affect the inversion process because the resulted parameters continuously remained appealing even to a 10% noise level (**Tables 5**, **6**). It can therefore be inferred that the new technique is intrinsically stable and demonstrates

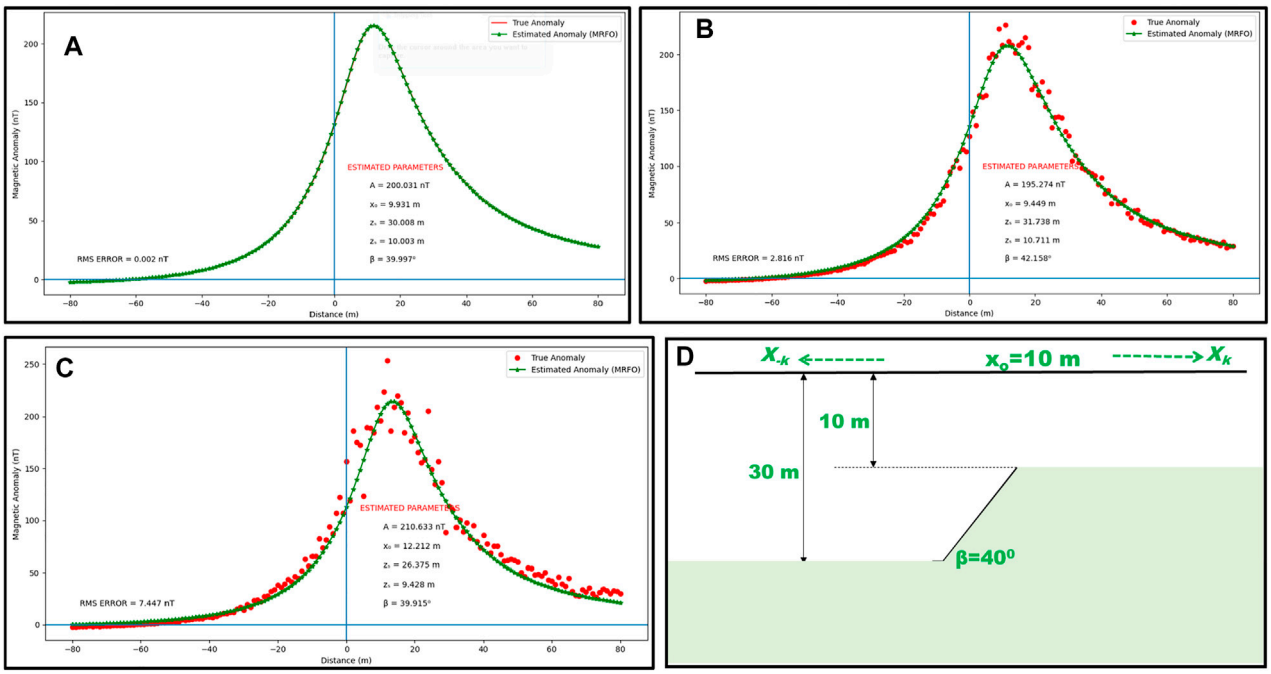

FIGURE 5 | Actual and estimated anomalies (magnetic) of a synthetic dipping fault structure with **(A)** 0% **(B)** 5% **(C)** 10% Gaussian noise using MRFO algorithm **(D)** Sketch of the fault model.

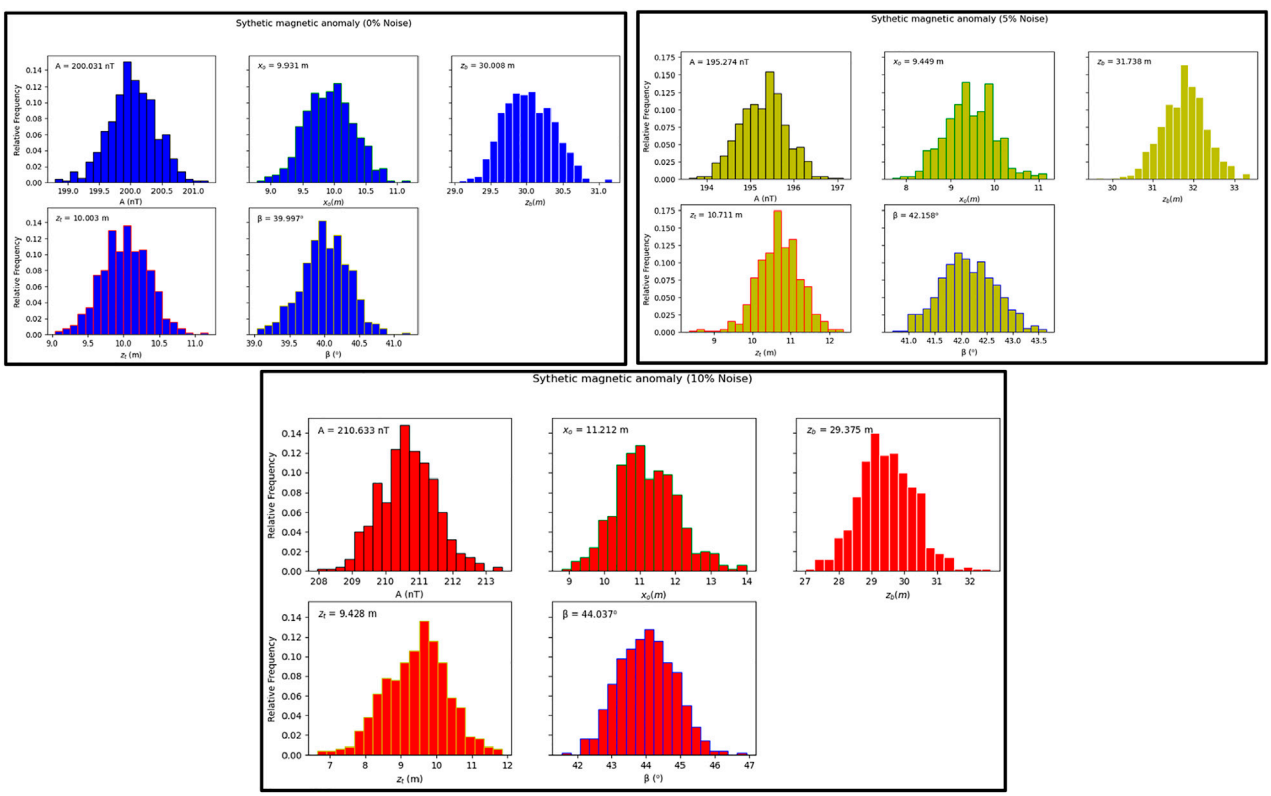

FIGURE 6 | Produced histograms after uncertainty appraisal using MCMC algorithm (synthetic magnetic anomaly). Estimated values indicated on upper-left part of the charts.

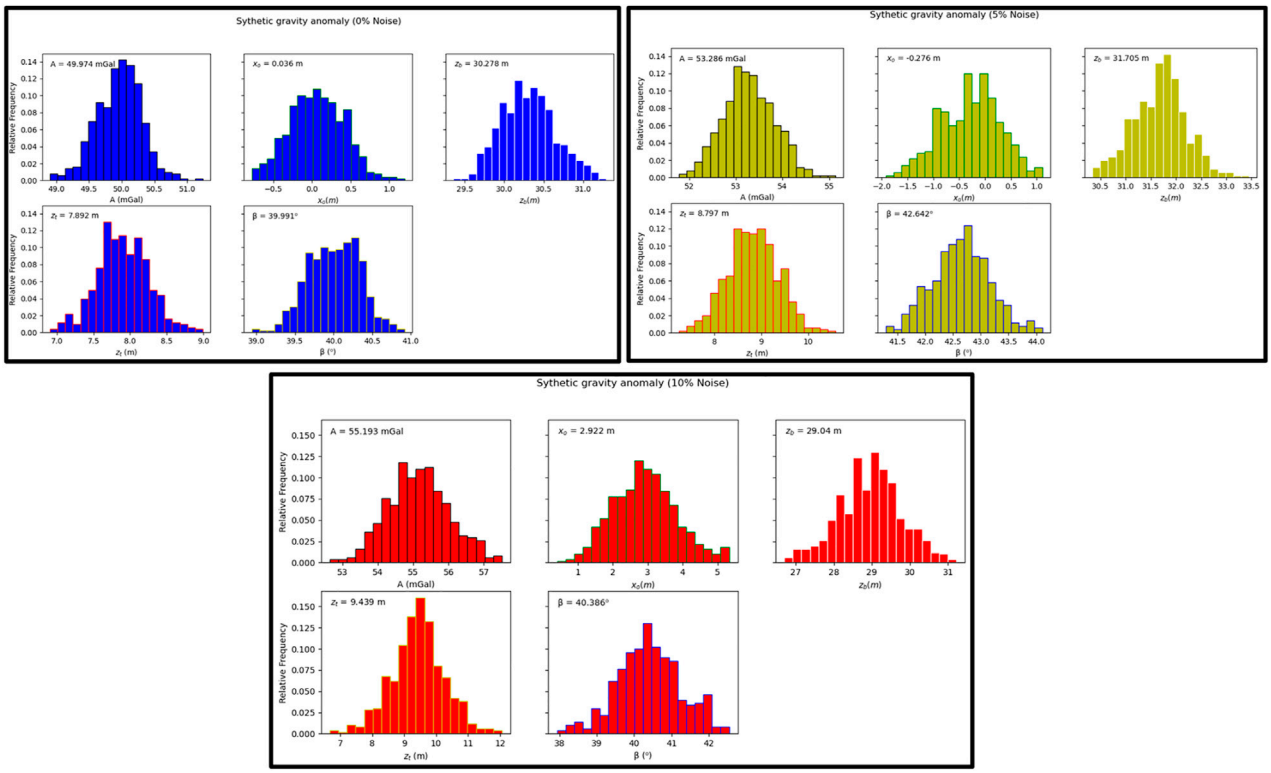

FIGURE 7 | Produced histograms after uncertainty appraisal using MCMC algorithm (synthetic gravity anomaly). Estimated values indicated on upper-left part of the chart.

TABLE 4 | Statistical results for RMS values obtained from parameter tuning of MRFO for synthetic gravity dataset.

S	RMS (mGal)		
	Minimum	Average	Standard deviation
0.5	0.4729	0.8468	0.0658
1	0.0374	0.0846	0.0173
1.5	0.0383	0.0519	0.0052
2	0.0063	0.0094	3.7841×10^{-8}
2.5	0.0327	0.0682	7.3081×10^{-5}
3	0.0472	0.0773	0.0401

TABLE 5 | Search bound, actual and estimated parameters synthetic gravity anomaly corrupted with random noise.

Model parameter	Percentage of noise and observed results	
—	5%	10%
A (mGal)	53.286	55.193
x_o (m)	–0.276	2.922
z_b (m)	31.705	29.040
z_t (m)	8.797	9.439
β (°)	42.642	40.386

commendable proficiency in handling corrupt anomaly data. **Figures 6**, **7** show the MCMC appraisal histogram for all noisy cases. Careful consideration of the generated histograms shows all estimated parameters as well-placed within excellent probability regions affirming the effectiveness of the algorithm's sampling operation.

FIELD CASES

It is generally understood that the strength and credibility of any new geophysical procedure depend on its practical applicability in the exploration of ores and minerals. The developed MRFO

TABLE 6 | Search space, actual and estimated parameters for synthetic magnetic anomaly corrupted with random noise.

Model parameter	Percentage of noise added and observed results	
—	5%	10%
A (nT)	195.274	210.633
x_o (m)	9.449	11.212
z_b (m)	31.738	29.375
z_t (m)	10.711	9.428
β (°)	42.158	44.037

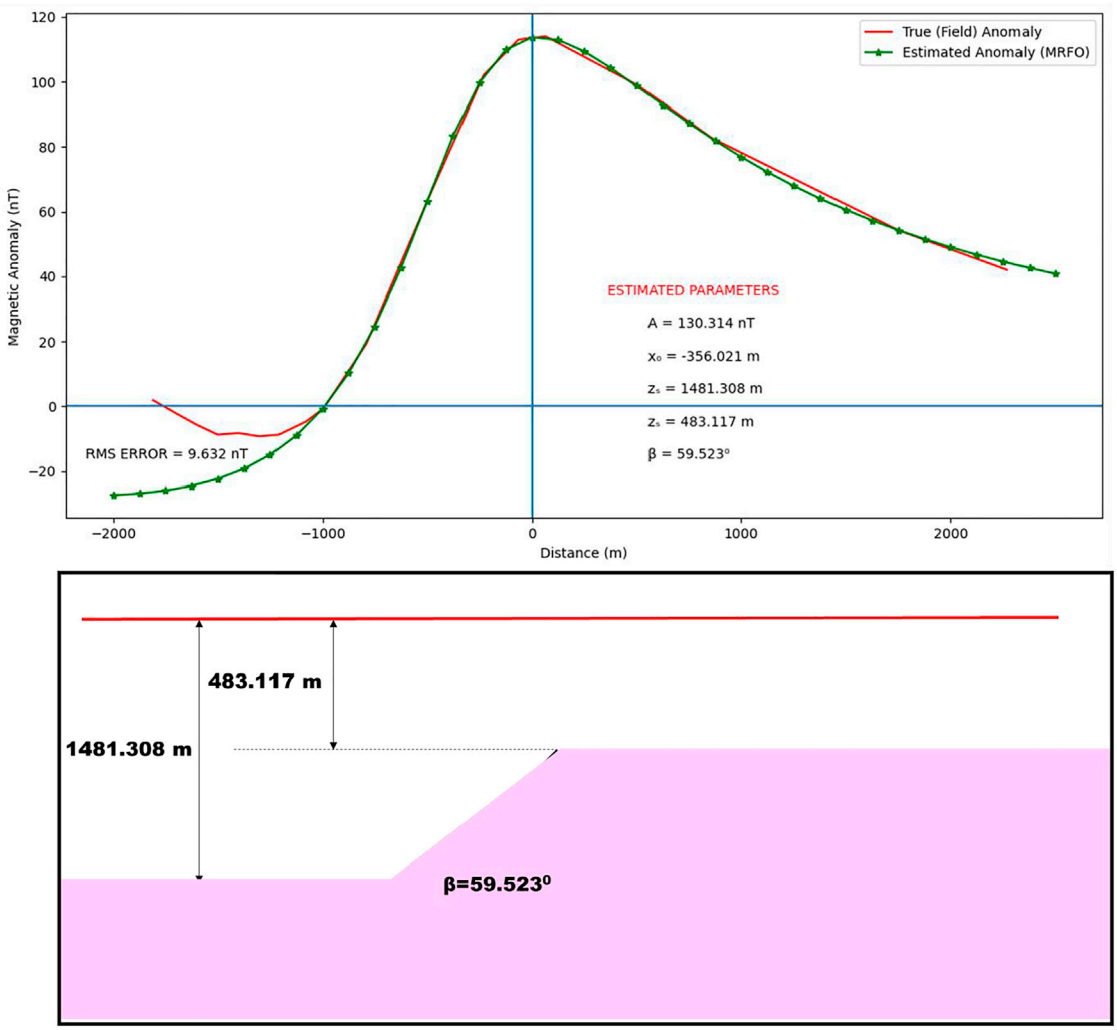

FIGURE 8 | Total magnetic anomaly of Lanchlan anomaly, Australia inverted using the MRFO procedure.

algorithm is as such, experimented against two real examples. The examples are taken from mining fields in the United States of America and Australia. The parameters reflecting the physical characteristics of the subsurface anomalies are estimated using the technique, and then subsequently compared against results from previous investigations for similar examples (published in the literature).

Lachlan Anomaly, Australia

In the first implementation of our new methodology with real-life anomalies, we seek at interpreting a total magnetic anomaly observed over the Molong anticlinorium; a major structural division of the Lachlan fold belt in New South Wales, Australia. The Lachlan fold belt is a middle Paleozoic accretionary orogen widely explored for its rich gold deposits. Orogenically, the belt was massively affected by the Benambrian Orogeny. The event is also believed to have resulted in the development of the Wagga-Omeo zone during the Late Ordovician to Early Silurian period. This was followed by the Middle Devonian Tabberabberan Orogeny which brought an end to the precratonic evolution; before it was being converted to a neo-craton at the last stage of the Carboniferous Kanimblan Orogeny. Structurally, the Silurian rocks which make up the belt fold characteristically to a syncline with a slight dip in the northwest direction (Wang et al., 2019). **Figure 8** is an east-west profile constructed from aeromagnetic data acquired over the anticlinorium with a flight height of about 200 m across the synclinal structure's western limb. The anomaly, buried at depth, was believed to be due to the abrupt thinning of the 1000 m thick tuff of the Douro volcanic against a fault (Ekinci et al., 2020). For this study, the 4 km long profile was digitized after every 125 m interval.

The MRFO technique was employed for parameterizing the subsurface structure, which is considered to be a dipping fault based on past geologic information. The parameter ranges indicated in **Table 7** are used to initialize the algorithm, and the maximum iterations allowed were pegged at 500. Finally, the RMS approach is used to monitor the difference between

TABLE 7 | Recovered parameter results and comparative analysis for Lanchlan Anomaly, Australia.

Model parameters	Search Space	Estimated (MRFO)	Qureshi & Nalaye (1978)	Ekinci et al. (2020)
A (nT)	0–1000	130.314	—	—
x_o (m)	−1500–1500	356.021	—	—
z_b (m)	1–4000	1481.308	1105	1149.84
z_t (m)	1–1000	483.117	115	135.81
β (°)	−180–180	59.523	49	138.27

the real and calculated data. The obtained results are displayed in **Table 7**.

The inversion result shows that the target structure is fault-like with an origin at approximately -356.021 m and an amplitude coefficient of 130.314 nT. The fault was inclined at 59.523° and is buried at 483.117 m to the top and 1481.308 m to the bottom of the fault. After 150 iterations, which lasted only 120 s, the iterations converged. This demonstrates that the MRFO algorithm performs admirably in terms of speed, complexity, and cost. Furthermore, the 9.632 nT misfit calculated implies that the actual and projected data fit together perfectly.

Several workers have shown interest in the Lachlan anomaly because of its economic potential, as evidenced by relevant literature. Qureshi & Nalaye (1978) decomposed the anomaly into symmetric and antisymmetric parts. Thereafter, after independently analyzing these two parts, they reported the buried feature as a fault dipping at an angle of 49° They also resulted 115 m as depth to the structure's top and 1105 m as depth to its bottom. Ekinci et al. (2020) alternatively inverted the anomaly using a fault model via differential evolution algorithm. Their experimentation resulted 1149.84 and 135.81 m as respective depths to the fault's bottom and top and 138.27° as dipping angle. It must be added that Ekinci et al. (2020) designed their forward models assuming non-coplanar relationships between the dislocated fault slabs. More too, their dipping angle was constructed to be strongly affected by the general strike and regional direction of magnetization. These factors are believed to have added up to the large dipping angle obtained from their study. However, the β-parameter from this study shows better favorability as it is compatible with observed dips for other structures in the region (35^0–80^0) as documented by the Geological Survey of South Wales (Qureshi & Nalaye, 1978). Nonetheless, analysis of these reports (**Table 7**) reveals that results from our new methodology still agree impressively with findings from similar studies in literature.

Garber Oil Field Anomaly, Oklahoma United States

Discovered in 1916, the Garber field which is situated on a dominant regional feature is one of Oklahoma's most prominent hydrocarbon fields (Kirkland et al., 1995; Gouin, 1956). The field is characterized by minor faults which dominate its surroundings and numerous anticlinal folds. In addition to these features, it is structurally deformed by the major Nemaha fault. In 1965, workers reported a fault structure suspected to be deep-seated from a geophysical contour map developed for the region (Ferris 1987). The suspected fault is the interpretative focus of this field example.

Gravity data was digitized across a 20-km-long profile over the fault structure. The sampling was carried out at 500 m intervals. To decipher the parameters defining the buried dipping fault structure, we followed the steps outlined in the proposed methodology. First, we initialized the algorithm with parameters based on the bounds shown in **Table 7**, as consistent with the previous field example. The maximum iteration number was then set to 500. The RMS error was used to monitor the disparity between the digitized gravity data and those calculated from MRFO-generated parameters (**Figure 9**). **Table 8** shows the results that were obtained.

According to results from the inversion process, the targeted source can be inferred as a fault-like structure inclined at an angle of 126.135°. Its origin is at a horizontal distance of 16.924 km on the profile. The depth to the structure's top and bottom is calculated to be 6.083 and 14.537 km respectively. The iterations converged after about 180 iterations, which took about 150 s, confirming the superiority of the algorithm in cost management and time complexity. More too, it is observed from the obtained error of 1.857 mGal that the measured and the computed data fit excellently (**Figure 9**).

Table 8 shows how the results obtained using our proposed methodology compare to those obtained using other methodologies and published in the literature. Using the least-squares inversion approach, Qureshi & Nalaye (1978) reported that the anomaly is a fault; with its top at a depth of 9.25 km and its bottom at a depth of 15.55 km. Murty et al. (2001) generalized an interpretation technique based on angular value decomposition. They then investigated the Garber field anomaly using the constructed tool. From results obtained after their analysis, they also pinpointed the anomaly to a fault structure. However, they reported the source structure as being relatively thinner and also as being buried at shallower top and bottom depths of 8.86 and 15.07 km. Using a comparative approach, Ekinci et al. (2019) recently employed the robust PSO and DE algorithms for the intelligent investigation of the Garber anomaly. They also confirmed that the anomaly-causing

TABLE 8 | Comparative analysis of parameter results for Garber Oil Field Anomaly, United States

Model parameters	Search Space	Estimated (MRFO)	Qureshi & Nalaye (1978)	Radhakrishna et al. (2001)	Ekinci et al. (2019)-PSO	Ekinci et al. (2019)-DE
A (mGal)	0–500	241.968	—	—	—	—
x_o (km)	0–20	16.924	—	—	—	—
z_b (km)	1–60	14.537	15.55	15.07	10.77	13.76
z_t (km)	1–30	6.083	9.25	8.86	5.62	5.10
β (°)	−180–180	126.135	—	—	108.41	141.13

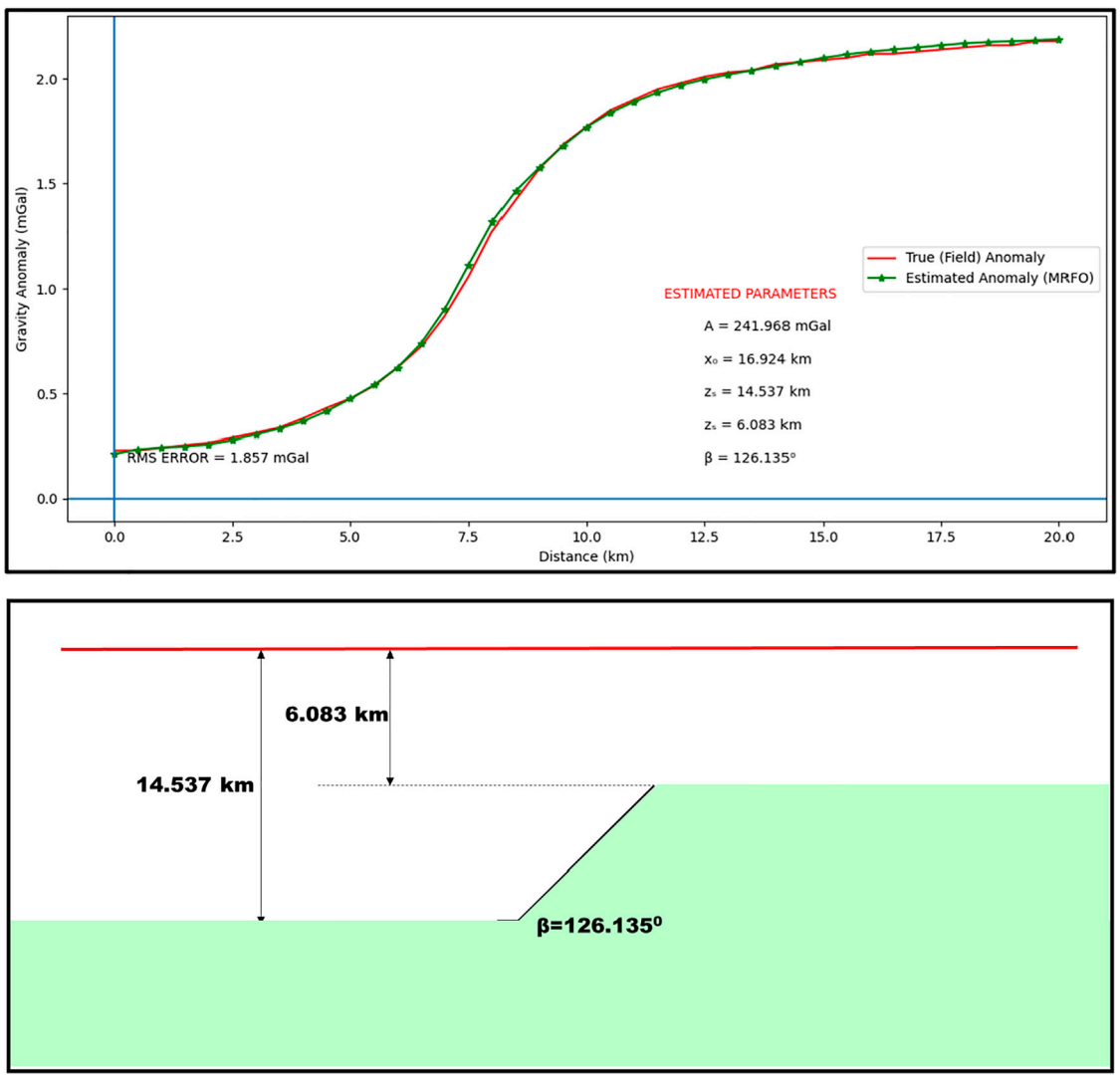

FIGURE 9 | Total gravity anomaly of Garber anomaly, Oklahoma inverted using the MRFO procedure.

structure was fault-like; howbeit, the fault was calculated as stretching from depth 5.62–10.77 km using PSO. DE resulted 5.10 and 13.76 km for the same respectively. These results indicate that findings obtained using our new methodology are consistent (**Table 8**) with existing information about this same anomaly, present in relevant literature.

DISCUSSION OF RESULTS

In both synthetic and actual examples, MRFO-based inversion proved to be an accurate and dependable technique for modeling potential field anomalies detected across geo-structures such as dipping faults (**Figures 10**, **11**). Furthermore, the MRFO

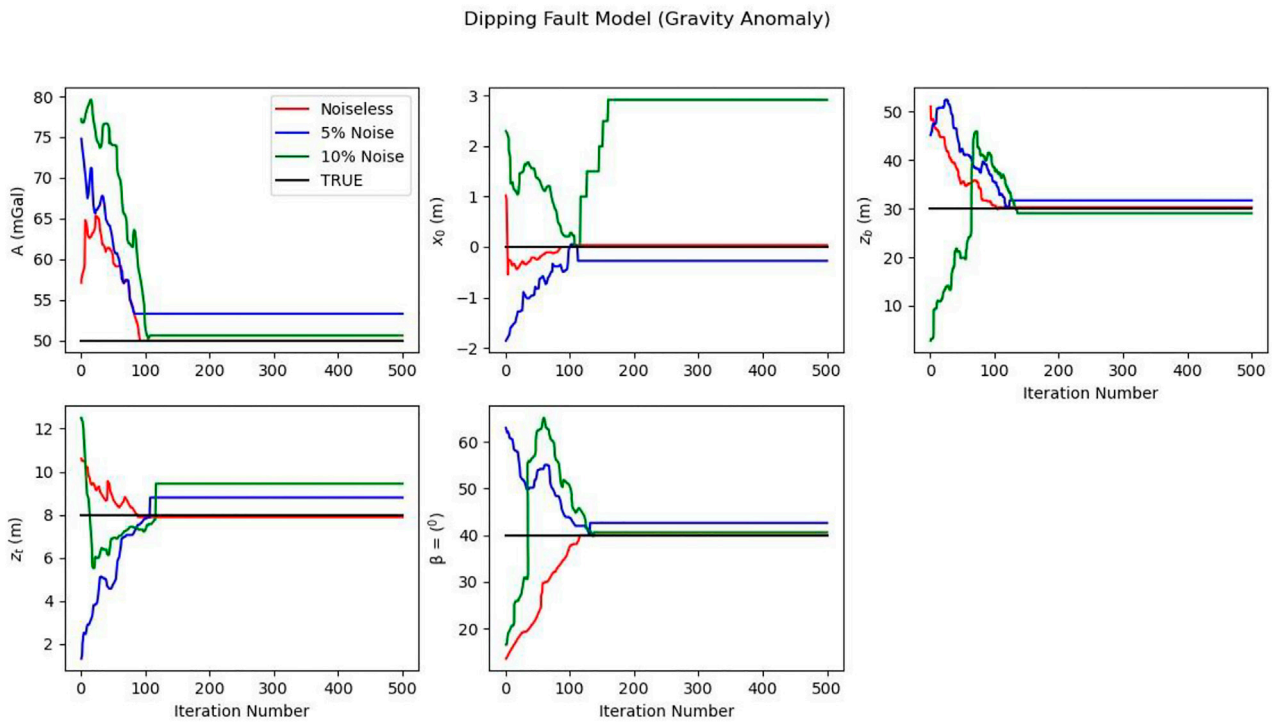

FIGURE 10 | Change in model parameters with iteration (Gravity Anomaly).

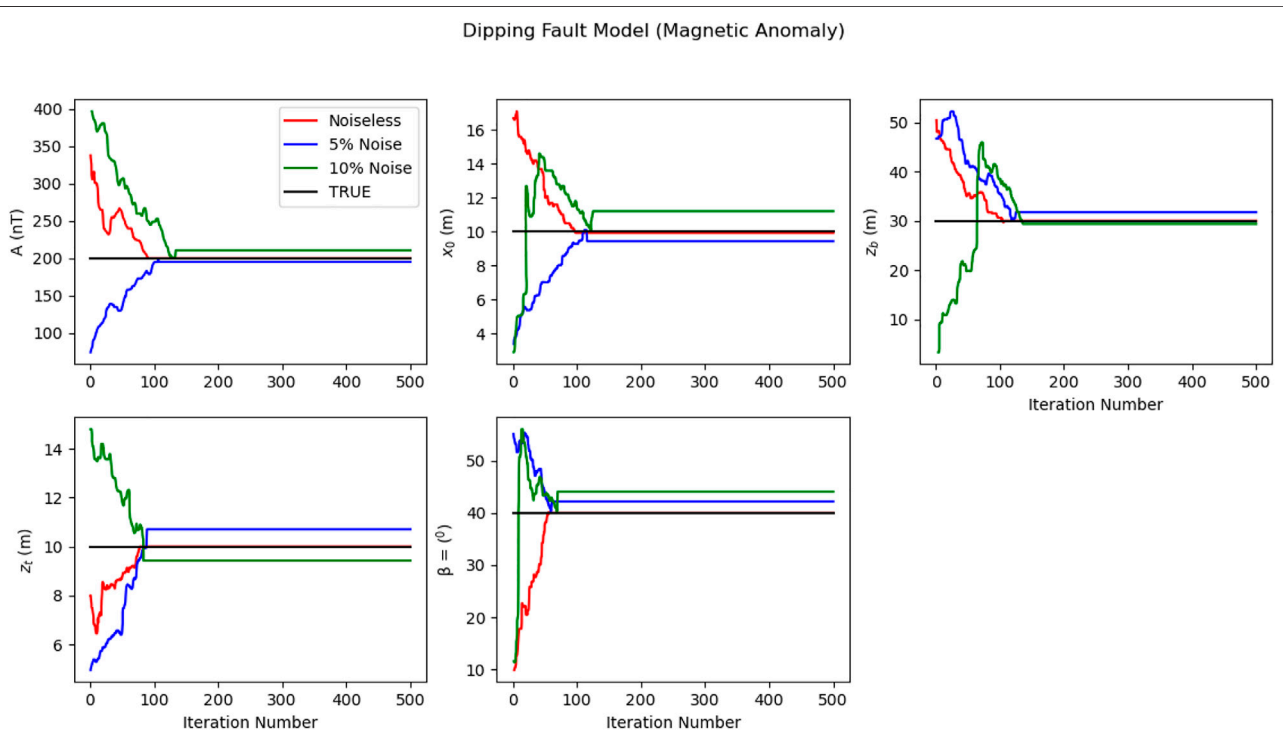

FIGURE 11 | Change in model parameters with iteration (Magnetic Anomaly).

algorithm's fast convergence rate suggests that it is a better-performing method for geophysical inversion. Surprisingly, this speed has no effect on optimization capability because the errors recorded at the end of the method are were still within acceptable ranges. Notably, the algorithm appears to overcome unpopular/recurring problems of immature convergence and local optima that regularly limits intelligent techniques such as ACO, PSO, and GA (Mehanee & Essa 2015; Roshan & Kumar Singh 2017; Chopard and omassini 2018; Izci et al., 2020; Hua et al., 2021). This is accomplished by the search agents' capacity to intelligently switch between chain and cyclone foraging techniques when necessary. The chain foraging method is often responsible for improving the algorithm's local search; whereas the cyclone strategy is mostly concerned with enhancing the algorithm's global search for solutions. By mutually combining the two–as the proposed methodology permits, a thorough exploration of the entire domain of the problem can be achieved. Noting these gains, as well as the comparatively lesser computational efforts required for the achievement of the gains, MRFO has been found to effectively supersede all other well-known optimizers in the resolution of the geophysical optimization problem. This is with respect to structural anomalies due to shallow and deep-seated dipping faults.

CONCLUSION

The feasibility of adapting the MRFO technique for the solution of geophysical inverse problems has been investigated. The procedure was structured towards obtaining precise estimates of five separate model parameters describing buried dipping fault. The parameters of interest were amplitude coefficient, origin, inclination, and depth from the surface to the top and bottom of the structural feature. The experimental data set consisted of synthetic potential field data that were later polluted with 5 and 10% random noise, as well as real profile anomalies extracted from mining fields in Australia and the United States. The algorithm execution rate was impressive-finding solutions with excellent RMS well before the maximum iterations allowed. Even so, analysis of the algorithm's performance and generated results reveal that the technique is outstanding, stable, and flexible, even in the presence of noise. The consistency of the results produced from the analysis of the field instances, when compared to control data generated from earlier research, further confirms that the procedure is accurate and reliable for the resolution of potential field problems. Resultantly, the approach is recommended for modeling potential field data and even alternative geophysical data such as self-potential, resistivity, and electromagnetics.

DATA AVAILABILITY STATEMENT

The raw data supporting the conclusion of this article will be made available by the authors, without undue reservation.

AUTHOR CONTRIBUTIONS

Conceptualization, AE; Data curation, UB; Formal analysis, O-IA and DG-O; Funding acquisition, KA; Investigation, UB, SE, and AA; Methodology, AA; Software, UB; Validation, O-IA; Visualization, SE and AE; Writing – review and editing, AE and AA.

ACKNOWLEDGMENTS

Deep thanks and gratitude to the Researchers Supporting Project number (RSP-2022/351), King Saud University, Riyadh, Saudi Arabia for funding this research article. The authors wish to thank the management of the University of Calabar for providing the facilities used for this research.

REFERENCES

Abbas, M. A., and Fedi, M. (2013). "Automatic DEXP Imaging of Potential fields Independent of the Structural Index," in 75th European Association of Geoscientists and Engineers Conference and Exhibition 2013 Incorporating SPE EUROPEC 2013: Changing Frontiers. doi:10.3997/2214-4609.20130120

Abdelrahman, E.-S., Gobashy, M., Abo-Ezz, E., and El-Araby, T. (2019). A New Method for Complete Quantitative Interpretation of Gravity Data Due to Dipping Faults. *Contrib. Geophys. Geodesy* 49, 133–151. doi:10.2478/congeo-2019-0007

Abdelrahman, E.-S. M., Abo-Ezz, E. R., and Essa, K. S. (2012). Parametric Inversion of Residual Magnetic Anomalies Due to Simple Geometric Bodies. *Exploration Geophys.* 43, 178–189. doi:10.1071/EG11026

Abo-Ezz, E. R., and Essa, K. S. (2016). A Least-Squares Minimization Approach for Model Parameters Estimate by Using a New Magnetic Anomaly Formula. *Pure Appl. Geophys.* 173, 1265–1278. doi:10.1007/s00024-015-1168-9

Alturki, F. A., Omotoso, H. O., Al-Shamma'a, A. A., Farh, H. M. H., and Alsharabi, K. (2020). Novel Manta Rays Foraging Optimization Algorithm Based Optimal Control for Grid-Connected PV Energy System. *IEEE Access* 8, 187276–187290. doi:10.1109/access.2020.3030874

Amoruso, A., Barba, S., Crescentini, L., and Megna, A. (2013). Inversion of Synthetic Geodetic Data for Dip-Slip Faults: Clues to the Effects of Lateral Heterogeneities and Data Distribution in Geological Environments Typical of the Apennines (Italy). *Geophys. J. Int.* 192, 745–758. doi:10.1093/gji/ggs042

Balkaya, Ç., Ekinci, Y. L., Göktürkler, G., and Turan, S. (2017). 3D Non-linear Inversion of Magnetic Anomalies Caused by Prismatic Bodies Using Differential Evolution Algorithm. *J. Appl. Geophys.* 136, 372–386. doi:10.1016/j.jappgeo.2016.10.040

Balkaya, Ç., and Kaftan, I. (2021). Inverse Modelling via Differential Search Algorithm for Interpreting Magnetic Anomalies Caused by 2D Dyke-Shaped Bodies. *J. Earth Syst. Sci.* 130. doi:10.1007/s12040-021-01614-1

Barnhart, W. D., and Lohman, R. B. (2010). Automated Fault Model Discretization for Inversions for Coseismic Slip Distributions. *J. Geophys. Res.* 115. doi:10.1029/2010JB007545

Ben, U. C., Akpan, A. E., Enyinyi, E. O., and Awak, E. (2021c). Novel Technique for the Interpretation of Gravity Anomalies over Geologic Structures with Idealized Geometries Using the Manta ray Foraging Optimization. *J. Asian Earth Sci. X* 6, 100070. doi:10.1016/j.jaesx.2021.100070

Ben, U. C., Akpan, A. E., Mbonu, C. C., and Ebong, E. D. (2021b). Novel Methodology for Interpretation of Magnetic Anomalies Due to Two-Dimensional Dipping Dikes Using the Manta Ray Foraging Optimization. *J. Appl. Geophys.* 192, 104405. doi:10.1016/j.jappgeo.2021.104405

Ben, U. C., Akpan, A. E., Mbonu, C. C., and Ufuafuonye, C. H. (2021a). Integrated Technical Analysis of Wind Speed Data for Wind Energy Potential Assessment in Parts of Southern and central Nigeria. *Clean. Eng. Tech.* 2, 100049. doi:10.1016/j.clet.2021.100049

Biswas, A., Parija, M., and Kumar, S. (2017). Global Nonlinear Optimization for the Interpretation of Source Parameters from Total Gradient of Gravity and Magnetic Anomalies Caused by Thin Dyke. *Ann. Geophys.* 60. doi:10.4401/ag-7129

Cerovský, I., and Pašteka, R. (2003). Imaging and Clustering of Depth Estimations for Werner and 2D-Euler Deconvolution. *Contrib. Geophys. Geodesy* 33, 2.

Chopard, B., and omassini, M. (2018). "Particle Swarm Optimization," *Natural Computing Series* (Cham: Springer). doi:10.1007/978-3-319-93073-2_6

Ekinci, S., Izci, D., and Hekimoğlu, B. (2021b). Optimal FOPID Speed Control of DC Motor via Opposition-Based Hybrid Manta Ray Foraging Optimization and Simulated Annealing Algorithm. *Arab J. Sci. Eng.* 46, 1395–1409. doi:10.1007/s13369-020-05050-z

Ekinci, S., Izci, D., and Kayri, M. (2021c). An Effective Controller Design Approach for Magnetic Levitation System Using Novel Improved Manta Ray Foraging Optimization. *Arab J. Sci. Eng.* doi:10.1007/s13369-021-06321-z

Ekinci, Y. L., Balkaya, Ç., and Göktürkler, G., 2020. Global Optimization of Near-Surface Potential Field Anomalies through Metaheuristics, 155, 188. doi:10.1007/978-3-030-28909-6_7

Ekinci, Y. L., Balkaya, Ç., Göktürkler, G., and Özyalln, Ş. (2021a). Gravity Data Inversion for the Basement Relief Delineation through Global Optimization: A Case Study from the Aegean Graben System, Western Anatolia, Turkey. *Geophys. J. Int.* 224 (2), 923–944. doi:10.1093/gji/ggaa492

Ekinci, Y. L., Balkaya, Ç., and Göktürkler, G. (2019). Parameter Estimations from Gravity and Magnetic Anomalies Due to Deep-Seated Faults: Differential Evolution versus Particle Swarm Optimization. *Turkish J. Earth Sci* 28 (6), 860–881. doi:10.3906/yer-1905-3

Elattar, E. E., Shaheen, A. M., Elsayed, A. M., and El-Sehiemy, R. A. (2020). Optimal Power Flow with Emerged Technologies of Voltage Source Converter Stations in Meshed Power Systems. *IEEE Access* 8, 166963–166979. doi:10.1109/ACCESS.2020.3022919

Essa, K. S., and Abo-Ezz, E. R. (2021). Potential Field Data Interpretation to Detect the Parameters of Buried Geometries by Applying a Nonlinear Least-Squares Approach. *Acta Geod Geophys* 56, 387–406. doi:10.1007/s40328-021-00337-5

Essa, K. S. (2021). Evaluation of the Parameters of the Fault-like Geologic Structure from the Gravity Anomalies Applying the Particle Swarm. *Environ. Earth Sci.* 80. doi:10.1007/s12665-021-09786-1

Essa, K. S. (2013). Gravity Interpretation of Dipping Faults Using the Variance Analysis Method. *J. Geophys. Eng.* 10, 015003. doi:10.1088/1742-2132/10/1/015003

Essa, K. S., Mehanee, S. A., and Elhussein, M. (2021). Gravity Data Interpretation by a Two-Sided Fault-like Geologic Structure Using the Global Particle Swarm Technique. *Phys. Earth Planet. Interiors* 311, 106631. doi:10.1016/j.pepi.2020.106631

Essa, K. S., and Munschy, M. (2019). Gravity Data Interpretation Using the Particle Swarm Optimisation Method with Application to mineral Exploration. *J. Earth Syst. Sci.* 128. doi:10.1007/s12040-019-1143-4

Essa, K. S., Nady, A. G., Mostafa, M. S., and Elhussein, M. (2018). Implementation of Potential Field Data to Depict the Structural Lineaments of the Sinai Peninsula, Egypt. *J. Afr. Earth Sci.* 147, 43–53. doi:10.1016/j.jafrearsci.2018.06.013

Fedi, M., and Florio, G. (2013). Determination of the Maximum-Depth to Potential Field Sources by a Maximum Structural index Method. *J. Appl. Geophys.* 88, 154–160. doi:10.1016/j.jappgeo.2012.10.009

Feng, J., Luo, X., Gao, M., Abbas, A., Xu, Y. P., and Pouramini, S. (2021). Minimization of Energy Consumption by Building Shape Optimization Using an Improved Manta-Ray Foraging Optimization Algorithm. *Energ. Rep.* 7, 1068–1078. doi:10.1016/j.egyr.2021.02.028

Ferris, C. (1987). Gravity Anomaly Resolution at the Garber Field. *Geophysics* 52, 1570–1579. doi:10.1190/1.1442275

Garabito, G., and Cruz, J. C. R. (2019). Application of Very Fast Simulated Annealing and Differential Evolution in the Search for FO-CRS Wavefield Attributes. *Geophysics* 84, O81–O92. doi:10.1190/geo2018-0193.1

Gharehchopogh, F. S., and Gholizadeh, H. (2019). A Comprehensive Survey: Whale Optimization Algorithm and its Applications. *Swarm Evol. Comput.* 48, 1–24. doi:10.1016/j.swevo.2019.03.004

Ghosh, K. K., Guha, R., Bera, S. K., Kumar, N., and Sarkar, R. (2021). S-shaped versus V-Shaped Transfer Functions for Binary Manta ray Foraging Optimization in Feature Selection Problem. *Neural Comput. Applic* 33, 11027–11041. doi:10.1007/s00521-020-05560-9

Gonzalez, S., Salvi, D., Baeza, D., Antonacci, F., and Sarti, A. (2021). A Data-Driven Approach to Violin Making. *Sci. Rep.* 11. doi:10.1038/s41598-021-88931-z

Gouin, F. (1956). Surface Criteria of Southern Oklahoma Oil Fields. *Pet. Geology. South. Okla*, 14–35. doi:10.1306/sv16348c1

Guo, Q., Ba, J., Luo, C., and Xiao, S. (2020). Stability-enhanced Prestack Seismic Inversion Using Hybrid Orthogonal Learning Particle Swarm Optimization. *J. Pet. Sci. Eng.* 192, 107313. doi:10.1016/j.petrol.2020.107313

Gupta, D. K., Gupta, J. P., Arora, Y., and Shankar, U. (2013). Recursive Ant colony Optimization: A New Technique for the Estimation of Function Parameters from Geophysical Field Data. *Near Surf. Geophys.* 11, 325–340. doi:10.3997/1873-0604.2012062

Hemeida, M. G., Ibrahim, A. A., Mohamed, A.-A. A., Alkhalaf, S., and El-Dine, A. M. B. (2021). Optimal Allocation of Distributed Generators DG Based Manta Ray Foraging Optimization Algorithm (MRFO). *Ain Shams Eng. J.* 12, 609–619. doi:10.1016/j.asej.2020.07.009

Houssein, E. H., Emam, M. M., and Ali, A. A. (2021). Improved Manta ray Foraging Optimization for Multi-Level Thresholding Using COVID-19 CT Images. *Neural Comput. Applic* 33, 16899–16919. doi:10.1007/s00521-021-06273-3

Hua, Y., Sui, X., Zhou, S., Chen, Q., Gu, G., Bai, H., et al. (2021). A Novel Method of Global Optimisation for Wavefront Shaping Based on the Differential Evolution Algorithm. *Opt. Commun.* 481, 126541. doi:10.1016/j.optcom.2020.126541

Hastings, W. K. (1970). Monte Carlo Sampling Methods Using Markov Chains and Their Applications. *Biometrika* 57 (1), 97–109. doi:10.1093/biomet/57.1.97

Izci, D., Ekinci, S., Eker, E., and Kayri, M. (2020). "Improved Manta Ray Foraging Optimization Using Opposition-Based Learning for Optimization Problems," in HORA 2020 - 2nd International Congress on Human-Computer Interaction, Optimization and Robotic Applications, Proceedings. doi:10.1109/HORA49412.2020.9152925

Kaftan, İ. (2017). Interpretation of Magnetic Anomalies Using a Genetic Algorithm. *Acta Geophys.* 65, 627–634. doi:10.1007/s11600-017-0060-7

Kanimozhi, V., and Jacob, T. P. (2019). Artificial Intelligence Based Network Intrusion Detection with Hyper-Parameter Optimization Tuning on the Realistic Cyber Dataset CSE-CIC-Ids2018 Using Cloud Computing. *ICT Express* 5, 211–214. doi:10.1016/j.icte.2019.03.003

Kirkland, D. W., Denison, R. E., and Rooney, M. A. (1995). Diagenetic Alteration of Permian Strata at Oil fields of South central Oklahoma, USA. *Mar. Pet. Geology.* 12 (6), 629–644. doi:10.1016/0264-8172(95)98089-N

Li, J., Li, J., Li, W., Jian, X., and Wu, X. (2020). Multi-scale Apparent Magnetization Inversion Imaging Method Based on the Theoretical Pseudo-gravity Anomalies. *Chaos, Solitons & Fractals* 131, 109480. doi:10.1016/j.chaos.2019.109480

Mbonu, C. C., Essiett, A. A., and Ben, U. C. (2021). Geospatial Assessment of Radiation hazard Indices in Soil Samples from Njaba, Imo State, South-Eastern Nigeria. *Environ. Challenges* 4, 100117. doi:10.1016/j.envc.2021.100117

Mehanee, S. A., and Essa, K. S. (2015). 2.5D Regularized Inversion for the Interpretation of Residual Gravity Data by a Dipping Thin Sheet: Numerical Examples and Case Studies with an Insight on Sensitivity and Non-uniqueness. *Earth Planet. Sp* 67. doi:10.1186/s40623-015-0283-2

Melo, F. F., and Barbosa, V. C. F. (2018). Correct Structural index in Euler Deconvolution via Base-Level Estimates. *Geophysics* 83, J87–J98. doi:10.1190/geo2017-0774.1

Metropolis, M. N., Rosenbluth, A. W., Rosenbluth, M. N., Teller, A. H., and Teller, E. (1953). Equation of State Calculations by Fast Computing Machines. *J. Chem. Phys.* 21 (6), 1087–1092.

Mosegaard, K., and Tarantola, A. (2002). 16 Probabilistic Approach to Inverse Problems. *Int. Geophys.* doi:10.1016/S0074-6142(02)80219-4

Mota, E. S. A., Medeiros, W. E., and Oliveira, R. G. (2020). Can Euler Deconvolution Outline Three- Dimensional Magnetic Sources? *Geophys. Prospecting* 68 (7), 2271–2291. doi:10.1080/20909977.2020.1743019

Murthy, I. R., Swamy, K. V., and Rao, S. J. (2001). Automatic Inversion of Magnetic Anomalies of Faults *Comput. Geosci.* 27 (3), 315–325.

Pan, J., Wang, X., Zhang, X., Xu, Z., Zhao, P., Tian, X., et al. (2009). 2D Multi-Scale Hybrid Optimization Method for Geophysical Inversion and its Application. *Appl. Geophys.* 6, 337–348. doi:10.1007/s11770-009-0034-x

Pilkington, M. (2006). Joint Inversion of Gravity and Magnetic Data for Two-Layer Models. *Geophysics* 71 (3), L35–L42. doi:10.1190/1.2194514

Qureshi, I. R., and Nalaye, A. M. (1978). A Method for the Direct Interpretation of Magnetic Anomalies Caused by Two-dimensional Vertical Faults. *Geophysics* 43, 179–188. doi:10.1190/1.1440819

Rezk, H., Mazen Alhato, M., Alhaider, M., and Bouall鏰ue, S. (2021). Fractional-Order Control of a Wind Turbine Using Manta Ray Foraging Optimization. *Comput. Mater. Continua* 68, 185–199. doi:10.32604/cmc.2021.016175

Roshan, R., and Singh, U. K. (2017). Inversion of Residual Gravity Anomalies Using Tuned PSO. *Geosci. Instrum. Method. Data Syst.* 6, 71–79. doi:10.5194/gi-6-71-2017

Russell, B. (2019). Machine Learning and Geophysical Inversion - A Numerical Study. *The Leading Edge* 38, 512–519. doi:10.1190/tle38070512.1

Scales, J. A., and Tenorio, L. (2001). Prior Information and Uncertainty in Inverse Problems. *Geophysics* 66, 389–397. doi:10.1190/1.1444930

Selem, S. I., Hasanien, H. M., and El-Fergany, A. A. (2020). Parameters Extraction of PEMFC's Model Using Manta Rays Foraging Optimizer. *Int. J. Energ. Res* 44, 4629–4640. doi:10.1002/er.5244

Sen, M. K., and Mallick, S. (2018). Genetic Algorithm with Applications in Geophysics. *Genet. Algorithm Appl. Geophys.*, 487–533. doi:10.1007/978-3-319-66532-0_7

Tarantola, A. 2005. *Inverse Problem Theory and Methods for Model Parameter Estimation*. Society for Industrial and Applied Mathematics. doi:10.1137/1.9780898717921

Turgut, O. E. (2021). A Novel Chaotic Manta-ray Foraging Optimization Algorithm for Thermo- Economic Design Optimization of an Air-Fin Cooler. *SN Appl. Sci* 3, 3. doi:10.1007/s42452-020-04013-1

Wang, D.-s., Wang, Z., Wang, Z.-q., Wang, G., Guo, X.-q., and Wu, Y.-d. (2019). Characteristics of Tectonic Deformation of the Melange Zone in the Lachlan Orogen along Eastern Coast of Australia. *China Geology.* 3, 1–16. doi:10.31035/cg2018131

Xie, W., Wang, Y.-C., Liu, X.-Q., Bi, C.-C., Zhang, F.-Q., Fang, Y., et al. (2019). Nonlinear Joint PP-PS AVO Inversion Based on Improved Bayesian Inference and LSSVM. *Appl. Geophys.* 16, 64–76. doi:10.1007/s11770-019-0750-9

Yadav, A., Yadav, K., and Anirbid Sircar, Anirbid. (2021). Feedforward Neural Network for Joint Inversion of Geophysical Data to Identify Geothermal Sweet Spots in Gandhar, Gujarat, India. *Energ. Geosci.* 2, 189–200. doi:10.1016/j.engeos.2021.01.001

Yusof, M. A., Agi, A., Gbadamosi, A., Junin, R., and Abbas, A. (2018). Uncertainty Analysis of Hydrocarbon in Place Calculation Using 3D Seismic and Well Data during Appraisal Stage - Case Study of Goldie Field, Offshore Sarawak. *J. Nat. Gas Sci. Eng.* 57, 238–265. doi:10.1016/j.jngse.2018.06.038

Zhao, W., Zhang, Z., and Wang, L. (2020). Manta ray Foraging Optimization: An Effective Bio-Inspired Optimizer for Engineering Applications. *Eng. Appl. Artif. Intelligence* 87, 103300. doi:10.1016/j.engappai.2019.103300

Zhdanov, M. S. (2002). *Geophysical Inverse Theory and Regularization Problems*. Amsterdam, Netherlands: Elsevier Science, Vol. 36.

Conflict of Interest: The authors declare that the research was conducted in the absence of any commercial or financial relationships that could be construed as a potential conflict of interest.

Publisher's Note: All claims expressed in this article are solely those of the authors and do not necessarily represent those of their affiliated organizations, or those of the publisher, the editors and the reviewers. Any product that may be evaluated in this article, or claim that may be made by its manufacturer, is not guaranteed or endorsed by the publisher.